Available online at www.sciencedirect.com
SCIENCE DIRECT®
Pergamon
Materials Research Bulletin 38 (2003) 395–407
Materials Research Bulletin
www.elsevier.com/locate/matresbu

Porous cobalt spheres for high temperature gradient magnetically assisted fluidized beds

James E. Atwater[a,*], James R. Akse[a], Goran N. Jovanovic[b], Richard R. Wheeler Jr.[a], Thana Sornchamni[b]

[a]*UMPQUA Research Company, P.O. Box 609, Myrtle Creek, OR 97457, USA*
[b]*Department of Chemical Engineering, Oregon State University, Corvallis, OR 97331, USA*

Received 21 October 2002; accepted 11 December 2002

Abstract

Porous metallic cobalt spheres have been prepared as high temperature capable media for employment in gradient magnetically assisted fluidization and filtration technologies. Cobalt impregnated alginate beads are first formed by extrusion of an aqueous suspension of Co_3O_4 into a Co(II) chloride solution. The organic polymer is thermally decomposed yielding cobalt oxide spheres, followed by reduction to the metallic state, and densification. Cobalt beads have been produced with porosities ranging between 10 and 50%, depending upon sintering conditions. The product media have been characterized by scanning electron microscopy (SEM), nitrogen adsorption porosimetry, and vibrating sample magnetometry.

Keywords: Magnetic materials; Metals; Chemical synthesis

1. Introduction

Fluidized bed contacting is a very effective method for conducting gas–solid and liquid–solid reactions, particularly those which are limited by mass transfer rates [1,2]. In fluidization, a dynamic balance is produced between drag, buoyancy, and gravitational forces. Maximum gas or liquid flow rates within fluidized bed reactors are limited by the fluid properties and also by the size and density distributions of the granular fluidization media. For a given gas–solid or liquid–solid system, higher rates of mass transfer can be achieved using magnetically stabilized fluidized bed (MSFB) methods which were pioneered by Rosensweig et al. [3–8]. In MSFB technology, magnetically susceptible solids are fluidized within a uniform magnetic field oriented parallel to the flow. Here, the magnetic forces between the particles

* Corresponding author. Tel.: +1-541-863-7770; fax: +1-541-863-7775.
E-mail address: jatwater@urcmail.net (J.E. Atwater).

0025-5408/03/$ – see front matter
doi:10.1016/S0025-5408(02)01072-3

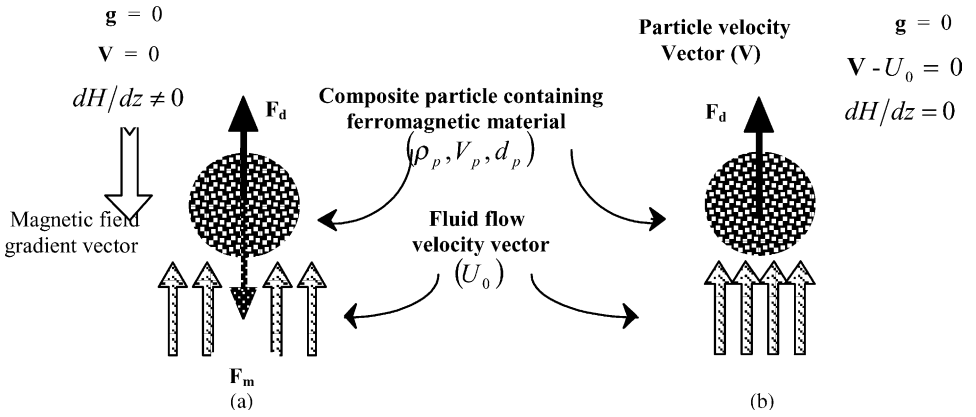

Fig. 1. Forces acting upon a ferromagnetic particle in zero gravity, (a) under a magnetic field gradient and (b) without an applied magnetic field. F_d—drag force, F_m—magnetic force.

augment the apparent size of the fluidization particles and thereby allow higher fluid flow rates under equivalent fluidization conditions. In recent years, fluidization phenomena [9–15], mass transfer rates [16,17], and fluid dynamics [18–20] of MSFB processes have been extensively studied.

Our research interest is in the application of magnetic forces acting upon sufficiently susceptible media to achieve both fluidization and filtration [21] in microgravity and hypogravity environments to facilitate solid waste gasification processes supporting NASA's long-term regenerative life support requirements for future extended duration manned space mission scenarios such as a Lunar base, Mars transit, and Mars base [22]. In the absence of a gravitational restoring force, conventional fluidization is not possible. However, using modified MSFB based methods in which magnetic field gradients are employed to produce additional force, liquid–solid fluidization can be achieved, as shown in Fig. 1. Using gradient magnetically assisted fluidized bed (GMAFB) methods this has been demonstrated in microgravity during two series of flight experiments aboard NASA's KC-135 aircraft [23].

In traditional MSFB systems, ferromagnetic particles are magnetized within a uniform magnetic field as in (1)

$$\boldsymbol{M} = \chi_{\mathrm{m}}\boldsymbol{H} \tag{1}$$

where the vectors $\boldsymbol{M}$ and $\boldsymbol{H}$ represent magnetization and magnetic field intensity, respectively, and χ_{m} is the magnetic susceptibility of the medium. The resulting magnetic flux density ($\boldsymbol{B}$) is given by,

$$\boldsymbol{B} = \mu_0(\boldsymbol{H} + \boldsymbol{M}) = \mu_0(\boldsymbol{H} + \chi_{\mathrm{m}}\boldsymbol{H}) = \mu\boldsymbol{H} \tag{2}$$

where μ_0 is the magnetic permeability of free space and $\mu = \mu_0(1 + \chi_{\mathrm{m}})$. The pole strength, p, of a magnetized ferromagnetic particle is related to the flux density by

$$\boldsymbol{B} = \frac{\mu}{4\pi}\frac{p}{r^2}\hat{\boldsymbol{i}} \tag{3}$$

where $\hat{\boldsymbol{i}}$ is a unit vector in the direction of the flux density. In the uniform magnetic field, forces are produced between the particles as in (4).

$$\boldsymbol{F} = \frac{\mu}{4\pi}\frac{p_1 p_2}{r^2}\hat{\boldsymbol{i}} \tag{4}$$

In (3) r is the distance from the pole at which $\boldsymbol{B}$ is measured, while in (4) r is the distance separating the two poles. In the gradient magnetically assisted fluidized bed (GMAFB) additional forces are produced through the application of a non-uniform magnetic field.

$$\boldsymbol{F} = \nabla(\boldsymbol{M} \cdot \boldsymbol{B}) \tag{5}$$

Using these additional forces, granular ferromagnetic media can be either fluidized or consolidated into a packed bed in the absence of gravity.

Gasification reactors necessarily require high temperature operating conditions, typically between 400 and 700 °C [24–26]. Because magnetic susceptibility is a strong function of temperature, it is important to utilize ferromagnetic media with a suitably high Curie temperature (T_c). This requirement eliminates nickel ($T_c = 358$ °C) and the ceramic ferrites from contention. While the suitability of iron ($T_c = 770$ °C) is marginal, the high temperature capability of cobalt ($T_c = 1120$ °C) renders it clearly superior to most other candidate materials.

In the current research, cobalt oxide impregnated cobalt alginate spheres were first prepared via an alginate gelation methodology [27–30]. The organic polymer was then thermally decomposed in an inert environment, resulting in cobalt oxide beads which were reduced to the metallic state under hydrogen. Densification of the spheres was achieved through further heat treatment. The relationships between sintering temperature, surface area, porosity, pore size distribution, and magnetic properties of the resulting materials were characterized by optical microscopy, SEM, nitrogen adsorption porosimetry, and vibrating sample magnetometry. The results of a preliminary investigation into the production of both metallic cobalt beads, and cobalt impregnated barium titanate beads have been reported previously [31].

2. Experimental

Spherical cobalt beads were prepared utilizing a four step process, including: (a) production of cobalt oxide impregnated polymeric spheres by alginate gelation, (b) oxidative and pyrolytic decomposition of the organic polymer, yielding cobalt oxide spheres, (c) reduction of cobalt to the zero-valent state, and (d) sintering of the metallic cobalt. An aqueous slurry was prepared containing 1.1% medium viscosity sodium alginate, 0.14% citric acid, 0.04% tannic acid, 2.45% ammonium hydroxide, and 13.75% cobalt oxide (Co_3O_4). The slurry was well mixed so that Co_3O_4 particles did not settle significantly during the gelation step. Droplets of the slurry were extruded through a 1 mm i.d. orifice, and allowed to fall into an aqueous 11.9% cobalt(II) chloride solution, where polymerization occurred via divalent cation promoted cross-linking reactions. The cobalt oxide impregnated cobalt alginate beads were aged in the $CoCl_2$ solution for 12 h, then thoroughly rinsed with deionized water and dried. This produced spherically symmetrical beads varying between 2 and 3 mm in diameter.

To decompose the alginate binder, the beads were heated under ambient air to 550 °C at a rate of 2 °C/min, and held at this temperature for 4 h in a tube furnace. The binder-free cobalt oxide beads were then reduced to cobalt metal using a 5% mixture of H_2 in N_2 at 550 °C. Following the complete reduction of cobalt oxide to cobalt metal, sintering runs to endpoint temperatures of 700, 800, 900, and 1000 °C were carried out to determine the thermal requirements for densification. In each case, the beads were heated from 550 °C to the final temperature under 5% hydrogen in nitrogen at 10 °C min^{-1}. The beads were held at the final temperature for 4 h, and then cooled to ambient temperature.

Grain sizes and porosities of the cobalt spheres were estimated by optical microscopy of polished cross-sections, using a linear point counting methodology. BET surface areas and pore size distributions were determined by nitrogen adsorption porosimetry. High resolution images of polished cross-sections and surfaces were acquired using a JEOL model JSM6300 XV scanning electron microscope. Magnetic properties of the material were characterized using a Lake Shore Model 7307 vibrating sample magnetometer.

3. Results and discussion

The time required for completion of the reduction step is strongly dependent on the gas flow rate. The cobalt beads are then densified in a sintering step. Sintering temperatures between 700 and 1000 °C were investigated. Most typically, sintering was accomplished in 240 min at a lower reducing gas flow rate to minimize temperature gradients within the tube furnace. The combined process produces highly porous and mechanically strong cobalt media. Numerous technical hurdles were overcome in the development of this process. To produce more than a few grams of cobalt beads at a time, improvements in the control of the alginate slurry rheology, strength of dried gelled beads, removal of alginate binder during thermal processing, and thermal process scale-up were required. The alginate-cobalt oxide formula was varied until stable and physically strong beads of ~1 mm diameter resulted. The reduction of cobalt oxide to cobalt metal required significant modification of the reaction conditions from those of the initial small scale experiments. With larger batches (i.e. 50–100 g), the reduction of cobalt oxide was limited by the availability of hydrogen in the reducing gas, since the maximum safe hydrogen content of the nitrogen process gas is 5%. For large batches, hydrogen became rapidly depleted by reduction reactions during the ramp up to sintering temperature, so that sintering temperatures were reached before complete

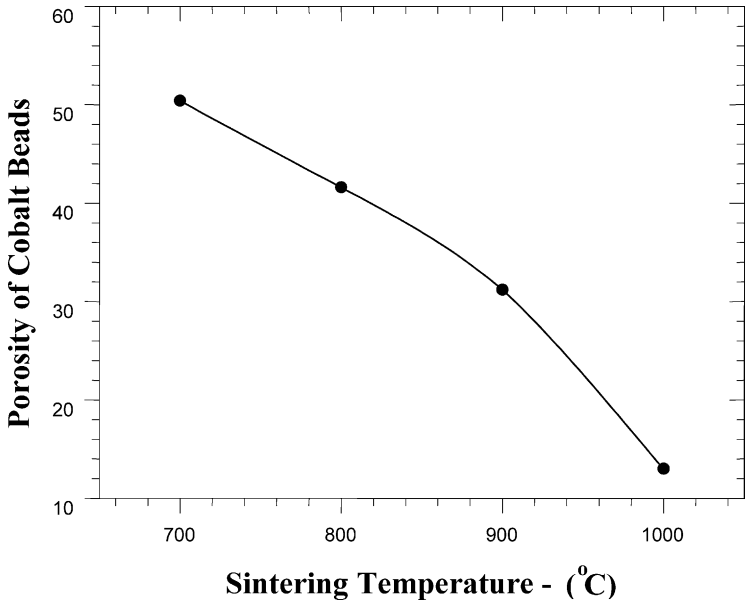

Fig. 2. Sintering temperature versus porosity of cobalt beads.

reduction of the cobalt oxide was achieved. This situation resulted in inconsistent sintering and densification within each batch. At this point, an attempt to substitute cobalt metal for cobalt oxide was made since cobalt metal does not require a reduction step. This proved unsuccessful due to the reaction of cobalt with water to produce cobalt oxide and a mixture of hydrogen and oxygen. Consequently, the

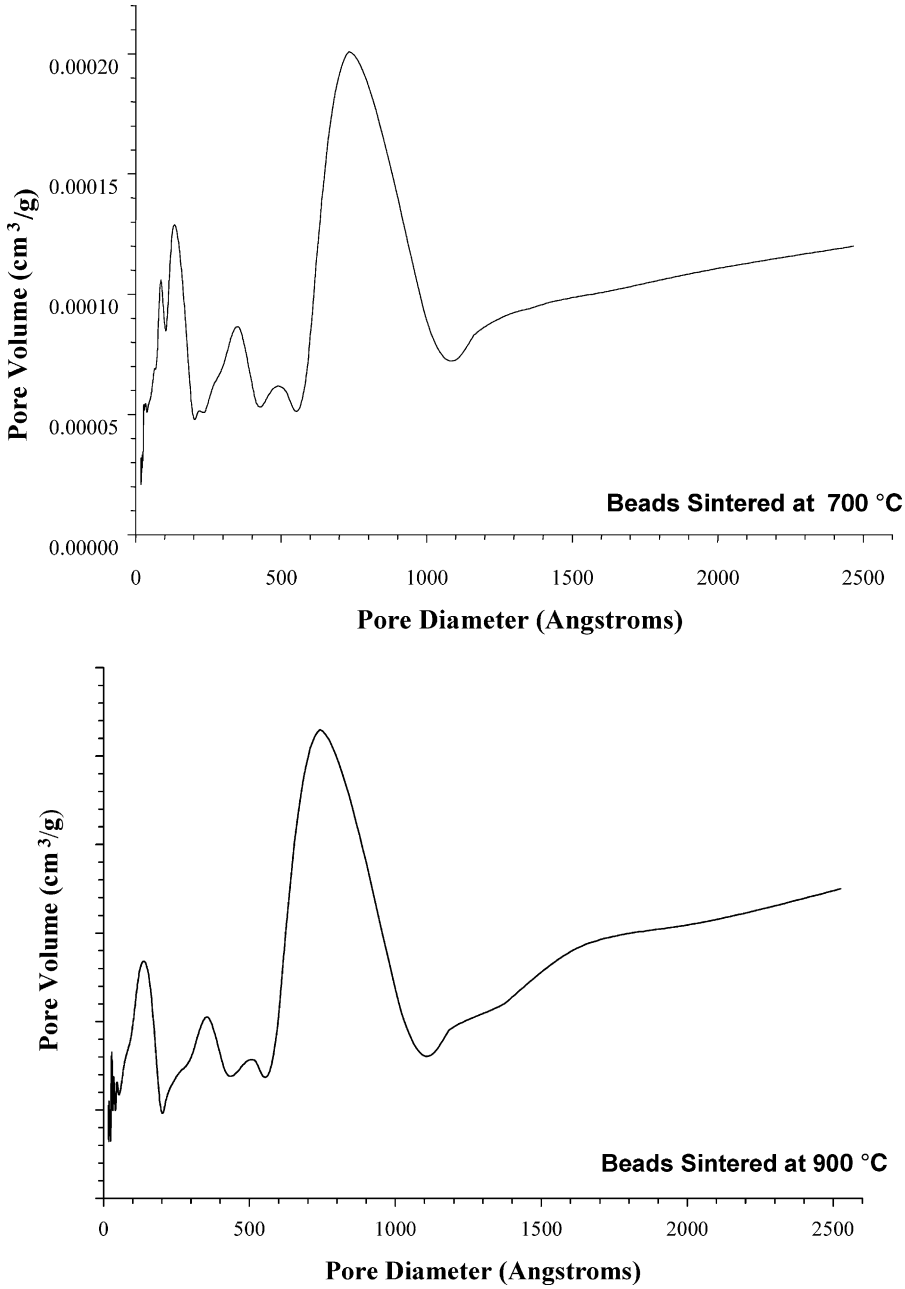

Fig. 3. Pore size distribution for cobalt beads sintered at 700 °C (top) and 900 °C (bottom).

original cobalt oxide reduction process was altered by providing longer reaction times and higher hydrogen/nitrogen gas flows at 550 °C to completely reduce cobalt oxide prior to the sintering step.

Following the complete reduction of cobalt oxide to cobalt metal, sintering runs to endpoint temperatures of 700, 800, 900, and 1000 °C were carried out to determine the thermal requirements for densification. In each case, the beads were heated from 550 °C to the final temperature under 5% hydrogen in nitrogen at 10 °C min^{-1}. The beads were held at the final temperature for 4 h, and then

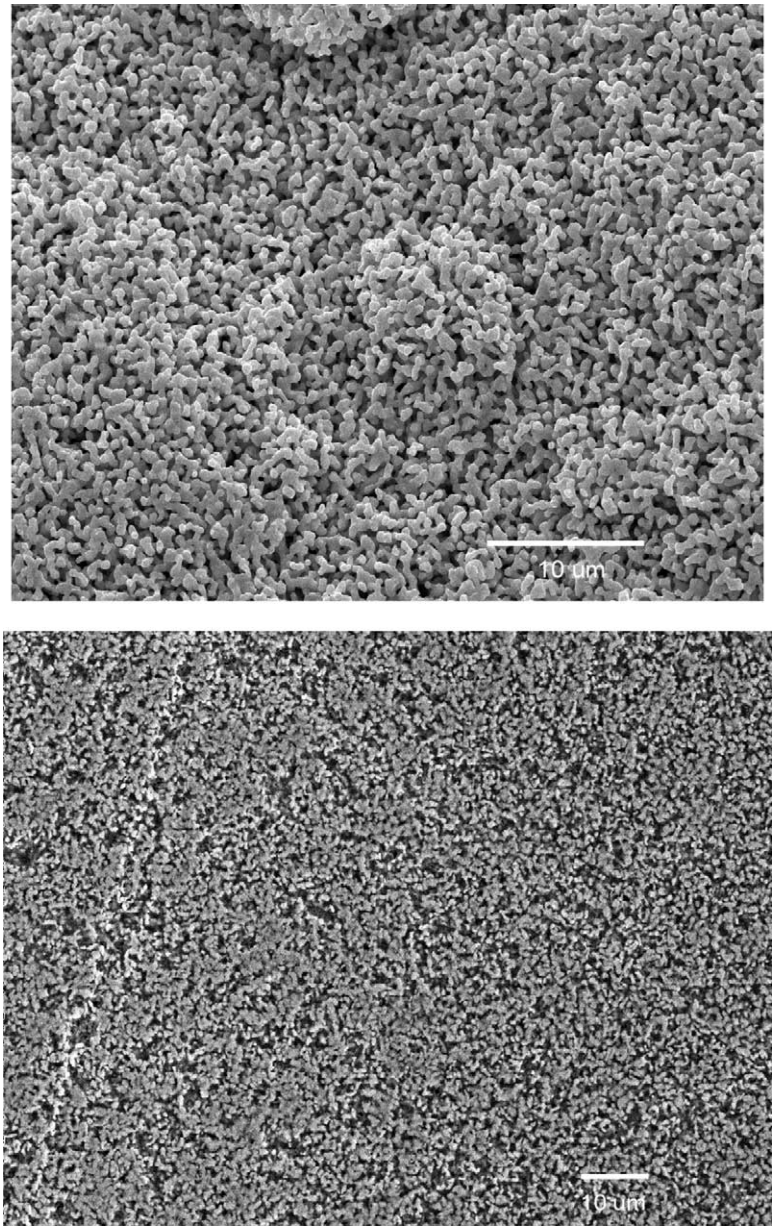

Fig. 4. Surface (top) and cross-section (bottom) SEM images of cobalt bead sintered at 700 °C.

cooled to ambient temperature at the maximum furnace cooling rate. Densities and porosities of the resulting cobalt beads were estimated utilizing a linear point count methodology. Bulk densities were 49.6, 58.4, 68.8, and 87.0% of theoretical for samples processed at 700, 800, 900, and 1000 °C, corresponding to porosities of 50.4, 41.6, 31.2, and 13.0%, respectively. The relationship between sintering temperature and bead porosity is shown in Fig. 2. Brunauer–Emmett–Teller (BET) surface

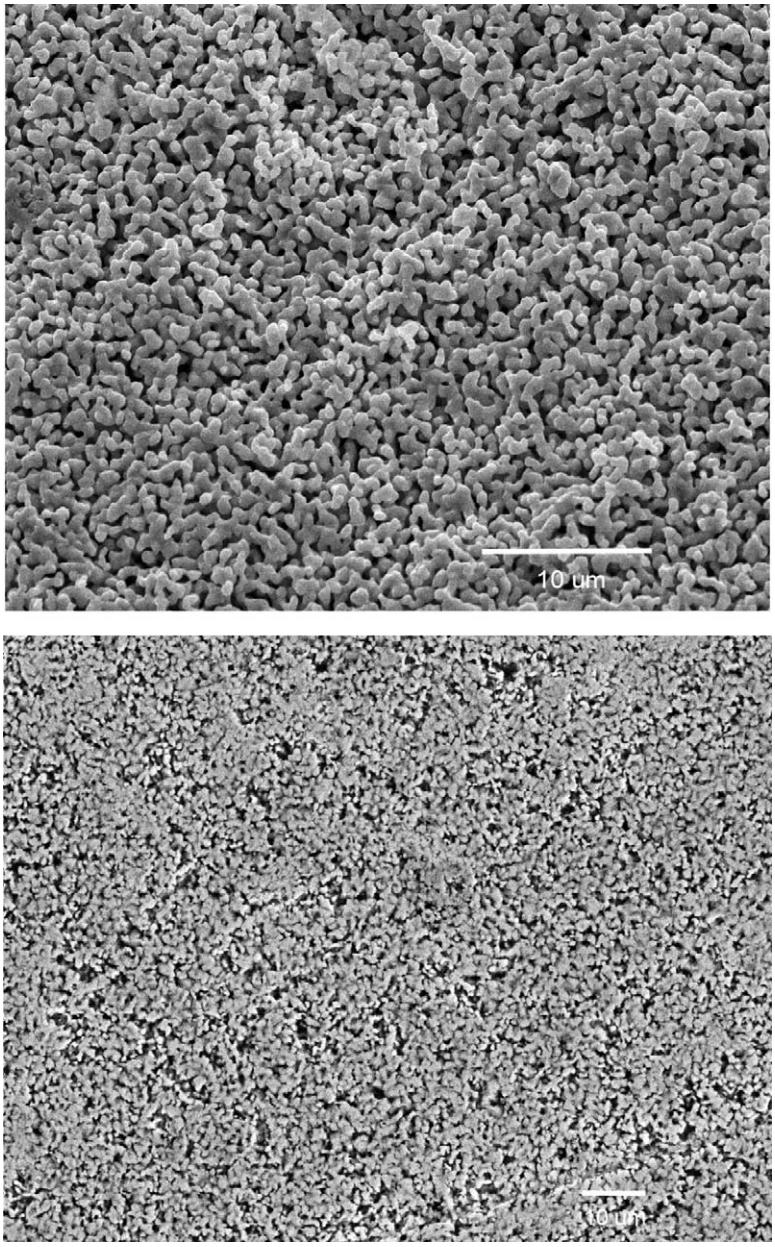

Fig. 5. Surface (top) and cross-section (bottom) SEM images of cobalt bead sintered at 800 °C.

areas and pore size distributions for samples sintered at 700 and 900 °C were characterized by nitrogen adsorption porosimetry. The resulting pore size distributions are shown in Fig. 3. A comparison of the results for cobalt spheres prepared at the two temperatures indicates that the relative distributions of pore diameters are similar but the absolute magnitudes are much greater for beads sintered at the lower temperature. This is in agreement with the observed general decrease in porosity with increasing

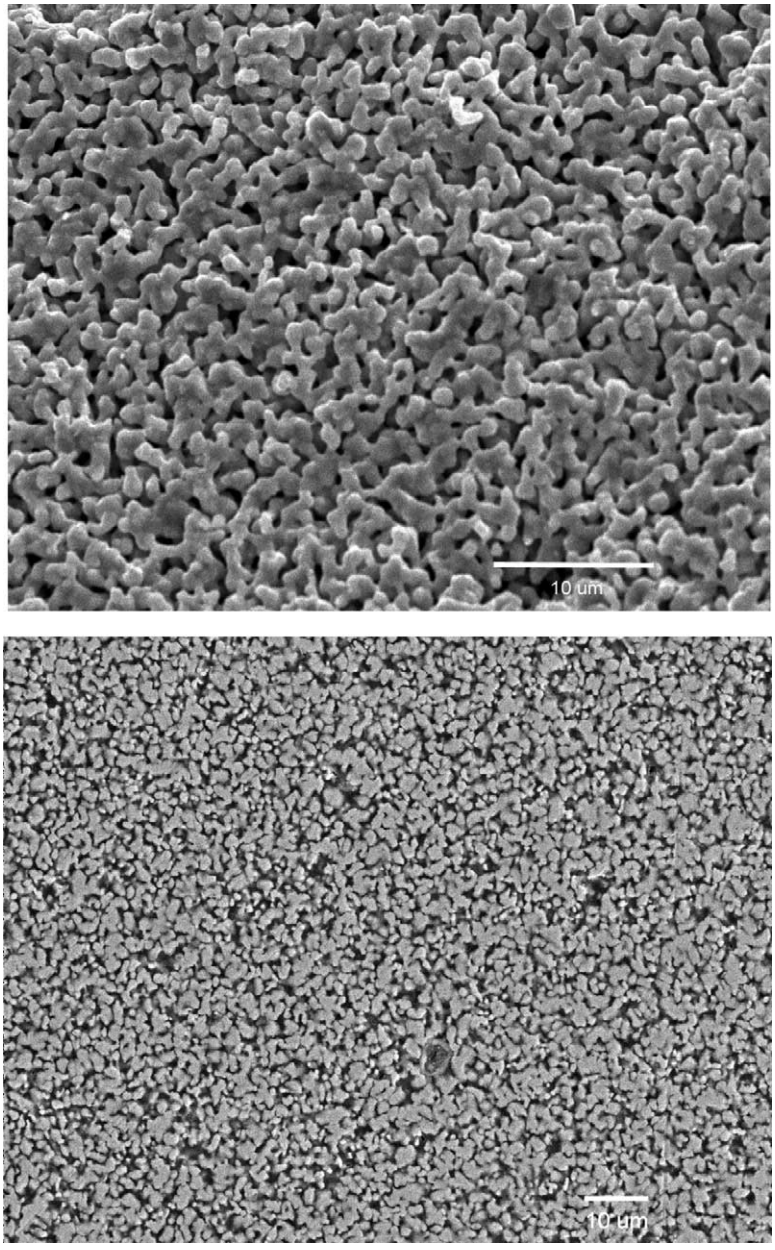

Fig. 6. Surface (top) and cross-section (bottom) SEM images of cobalt bead sintered at 900 °C.

sintering temperature. BET surface areas were 1.24 and 0.639 m^2/g, for cobalt beads densified at 700 and 900 °C, respectively.

Scanning electron photomicrographs taken at 2500× magnification for both the cobalt bead surfaces and polished cross-sections of samples fired at these temperatures are shown in Figs. 4–7, respectively. At the lowest sintering temperature, the reduction of the sub-micron cobalt oxide powder resulted in a

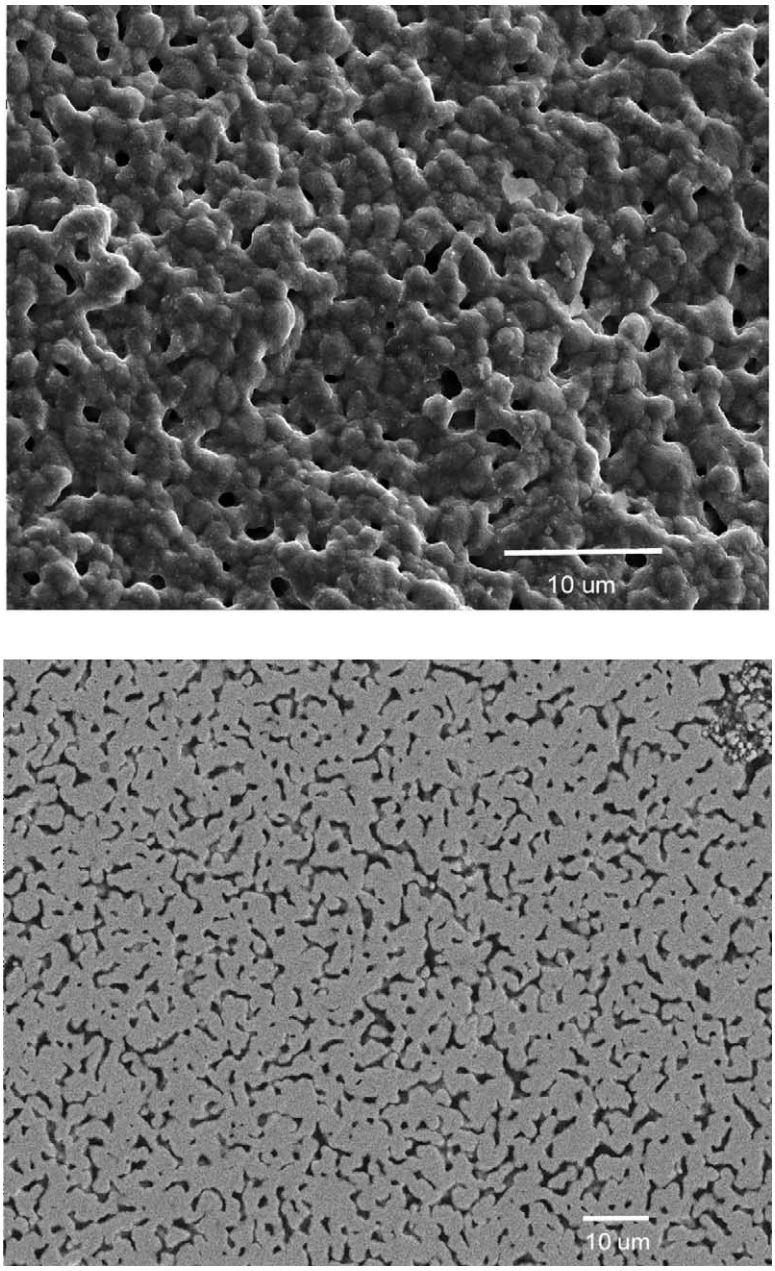

Fig. 7. Surface (top) and cross-section (bottom) SEM images of cobalt bead sintered at 1000 °C.

Table 1
Summary of magnetic properties of beads sintered at temperatures between 700 and 1000 °C

T (°C)	M_s		M_r		H_c	
	A/m	emu/cm^3	A/m	emu/cm^3	A/m	Oe
700	6.4×10^5	6.4×10^2	4.46×10^3	4.46	5.47×10^3	68.7
800	8.2×10^5	8.2×10^2	3.81×10^3	3.81	4.55×10^3	57.2
900	7.1×10^5	7.1×10^2	2.29×10^3	2.29	4.45×10^3	55.9
1000	1.26×10^6	1.26×10^3	1.55×10^2	0.155	5.2×10^2	6.53

loosely connected metal compact with an average grain size of ~0.5 μm. The higher thermal treatment temperature of 800 °C increased the grain sizes to ~1 μm. Both of these samples were mechanically weak, and therefore, unsuitable for use in a gasification reactor. At 900 °C, the grain size increased to between 1.5 and 2 μm. Beads produced at this temperature were mechanically robust and relatively dense (6.12 g/cm^3). The grain size in the beads processed at 1000 °C increased to between 2 and 3 μm.

The magnetic properties of these beads were studied using a vibrating sample magnetometer. Test results are summarized in Table 1. Room temperature magnetization–demagnetization curves for beads sintered at 700, 800, 900, and 1000 °C are shown in Figs. 8–11, respectively. All cobalt beads exhibited strong magnetic susceptibility and very little hysteresis, indicating low remnant magnetization (M_r). Coercive field strengths ranged between 6.53 and 68.7 Oe. The saturation volumetric magnetization (M_s) increased from 647 emu/cm^3 at the sintering temperature of 700 °C to 1261 emu/cm^3 at 1000 °C,

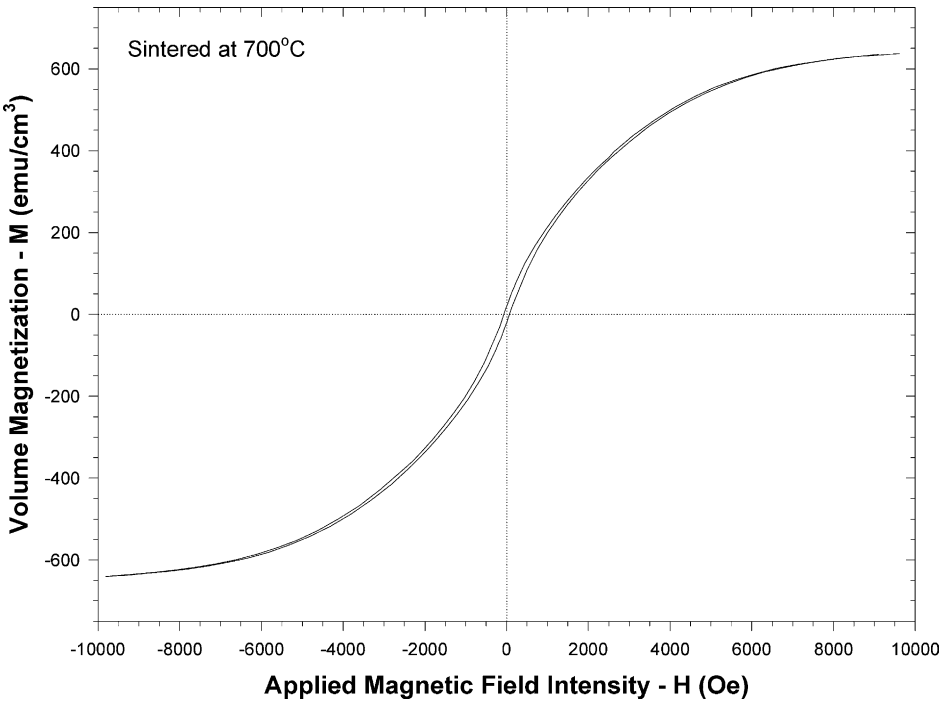

Fig. 8. Magnetization–demagnetization curves for cobalt beads sintered at 700 °C.

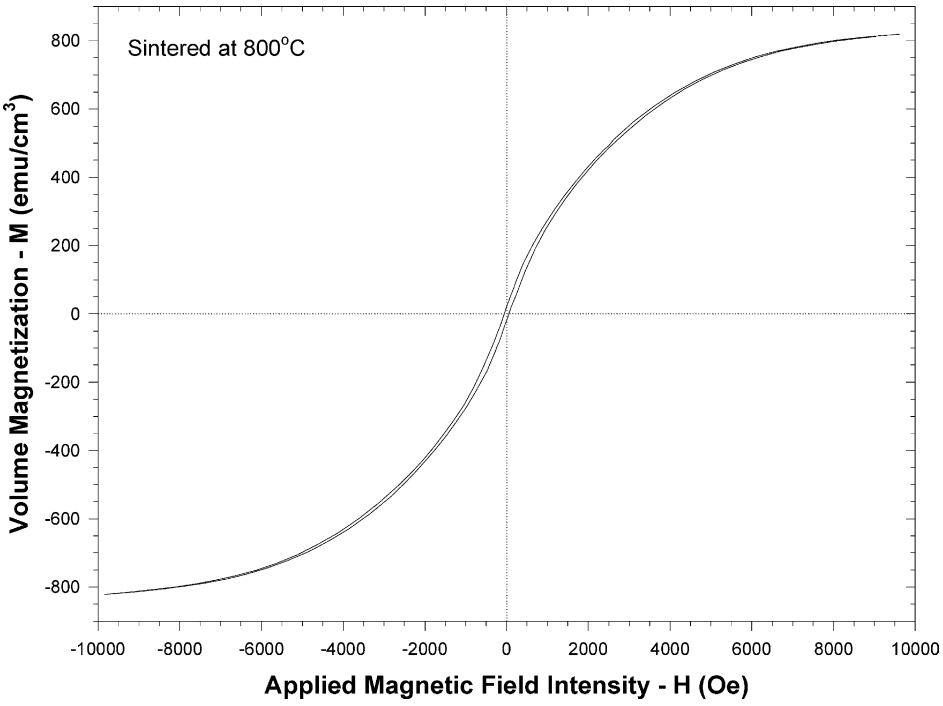

Fig. 9. Magnetization–demagnetization curves for cobalt beads sintered at 800 °C.

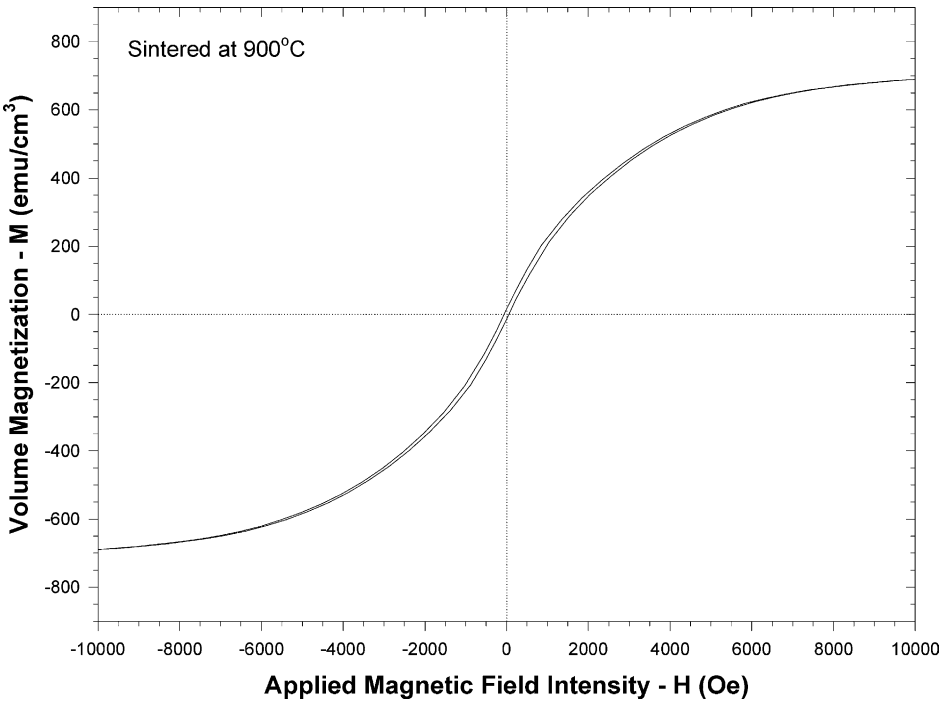

Fig. 10. Magnetization–demagnetization curves for cobalt beads sintered at 900 °C.

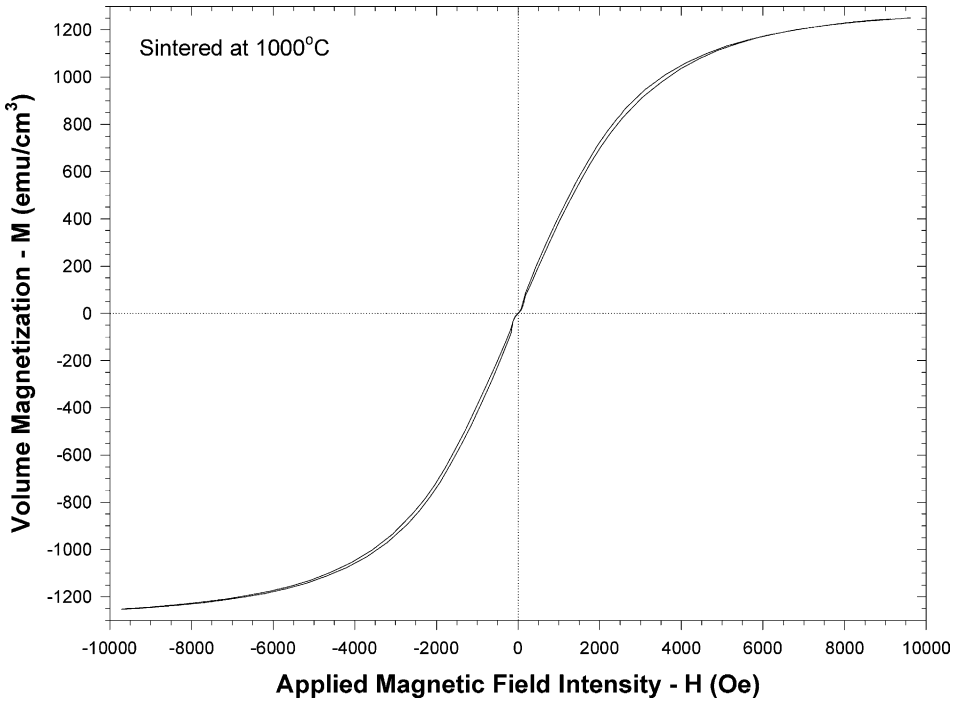

Fig. 11. Magnetization–demagnetization curves for cobalt beads sintered at 1000 °C.

correlating with increased densification. The beads prepared at 900 °C were anomalous in this respect, showing somewhat lower saturation magnetization than would be expected based upon the metallic cobalt content of the beads. However, these beads still showed very strong magnetic susceptibility. Magnetization–demagnetization experiments using the beads prepared at 900 °C were repeated, yielding equivalent results. Given the volumetric saturation magnetization of 1422 emu/cm^3 for pure cobalt metal with no porosity at 20 °C, it is evident that the ferromagnetic properties of the porous cobalt beads produced in this study generally correlate with the bulk densities of the materials and their cobalt contents on a volumetric basis.

Based upon these results, a sintering temperature of 900 °C was selected for the production of media in quantities to support both laboratory and flight experiments. Media prepared under these conditions exhibit good mechanical strength and sufficient porosity. In subsequent runs, after 4 h at 900 °C, a reproducible density of 5.61 g/cm^3 was achieved, with bead diameters varying between 1 and 1.2 mm. These beads were mechanically strong and retained interconnected porosity. This combination provides the physical robustness necessary for employment in a fluidized bed reactor at elevated temperature with the surface area and porosity characteristics required for catalytic activity.

Acknowledgements

This work was funded by the Office of Physical and Biological Research of the National Aeronautics and Space Administration under grant NAG9-1181. The authors thank John W. Fisher at NASA—Ames

Research Center for his helpful suggestions and support and Dr. David C. Johnson of the Materials Science Institute at the University of Oregon for technical assistance.

References

[1] O. Levenspiel, Chemical Reaction Engineering, Wiley, New York, 1972.
[2] D. Kunii, O. Levenspiel, Fluidization Engineering, Butterworth-Heinemann, Boston, 1991.
[3] R.E. Rosensweig, Ferrohydrodynamics, Cambridge University Press, New York, 1985.
[4] R.E. Rosensweig, J.H. Siegell, W.K. Lee, T. Mikus, AIChE Symp. Ser. 77 (1981) 8.
[5] R.E. Rosensweig, Science 204 (1979) 57.
[6] R.E. Rosensweig, Ind. Eng. Chem. Fundam. 18 (1979) 260.
[7] R.E. Rosensweig, G.R. Jerauld, M. Zahn, in: O. Brulin, R.K.T. Hsieh (Eds.), Continuum Models of Discrete Systems 4, North-Holland, New York, 1981, pp. 137–144.
[8] R.E. Rosensweig, M. Zahn, W.K. Lee, P.S. Hagan, in: R.E. Meyer (Ed.), Theory of Dispersed Multiphase Flow, Academic Press, New York, 1983, pp. 359–384.
[9] M.A. Burns, D.J. Graves, Chem. Eng. Commun. 67 (1988) 315.
[10] L.M. Sajc, Z.R. Jovanovic, G.V. Novakovic, G.N. Jovanovic, R.D. Pesic, D.V. Vucovic, Trans. IChemE 72 (1994) 236.
[11] G.N. Jovanovic, L.M. Sajc, Z.R. Jovanovic, G.V. Novakovic, B. Kundacovic, B. Obradovic et al., J. Serb. Chem. Soc. 57 (1992) 345.
[12] G.N. Jovanovic, L. Sajc, Z.R. Jovanovic, B. Bugarski, G.V. Novakovic, J. Serb. Chem. Soc. 61 (1996) 319.
[13] T.T. Ames, R.M. Worden, Biotechnol. Prog. 13 (1997) 336.
[14] M.J. Rhodes, X.S. Wang, K.S. Gan, S. Phadtajaphan, Chem. Eng. Sci. 56 (2001) 5429.
[15] Y.-C. Lin, L.-P. Leu, Powder Technol. 120 (2001) 199.
[16] M. Franzreb, R. Hausmann, C. Hoffmann, W.H. Holl, React. Polym. 46 (2001) 247.
[17] M. Al-Mulhim, Enhancement of Mass Transfer Coefficient in a Magnetically Stabilized Liquid–Solid Fluidized Bed, M.S. Thesis, Oregon State University, Corvallis, Oregon, 1995.
[18] C.-M. Chen, L.-P. Leu, Powder Technol. 117 (2001) 198.
[19] D. Bohm, B. Pittermann, Chem. Eng. Technol. 23 (2000) 309.
[20] L. Honerez, Fluid Dynamic Characteristics of a Magnetically Stabilized Liquid–Solid Fluidized Bed, M.S. Thesis, Oregon State University, Corvallis, Oregon, 1994.
[21] T. Abbasov, Powder Technol. 115 (2001) 215.
[22] J.E. Atwater, J.R. Akse, J.L. DeHart, G.N. Jovanovic, T. Sornchamni, S. Yoo, J.W. Fisher, SAE Tech. Paper Ser. 1999-01-2183 (1999) 1.
[23] T. Sornchamni, The Prediction of Voidage Distribution in a Non-uniform Magnetically Assisted Fluidized Bed: Theory and Experiment, M.S. Thesis, Oregon State University, Corvallis, Oregon, 2000.
[24] G. Schuster, G. Loffler, K. Weigl, H. Hofbauer, Bioresource Technol. 77 (2001) 71.
[25] J.M. Encinar, F.J. Beltran, A. Ramiro, J.F. Gonzalez, Fuel Process. Technol. 55 (1998) 219.
[26] L. Garcia, M.L. Salvador, J. Aruzo, R. Bilbao, Fuel Process. Technol. 69 (2001) 157.
[27] C.D. Gilson, A. Thomas, J. Chem. Technol. Biotechnol. 62 (62) (1995) 227.
[28] G.T. Grant, E.R. Morris, D.A. Rees, P.J.C. Smith, D. Thom, FEBS Lett. 32 (1973) 195.
[29] A. Haug, Composition and Properties of Alginates, Report No. 30, Norwegian Institute of Seaweed Research, Trondheim, Norway, 1964.
[30] H.L. Huguet, A. Groboillot, R.J. Neufeld, D. Poncelet, E. Dellacherie, J. Appl. Polym. Sci. 51 (1994) 1427.
[31] J.E. Atwater, J.R. Akse, G.N. Jovanovic, T. Sornchamni, J. Mater. Sci. Lett. 20 (2001) 487.